Journal of Marine Research, 53, 1025–1057, 1995

The growth of convective plumes at seafloor hot springs

by Kevin G. Speer[1] and John Marshall[2]

ABSTRACT

The growth of buoyant plumes in the presence of stratification (N) and rotation (f) is studied and illustrated with a number of numerical experiments of convection induced by a localized source of buoyancy at the lower boundary of a linearly stratified fluid. The presence of stratification constrains the convection in the vertical giving rise to an equilibrium-spreading layer which receives the rising mass of plume fluid; the plume can be divided into an upper, mass-source driven anticyclone and a lower, buoyancy-source (F) driven cyclone. With N/f large, the plume's rise-height is set by the classical non-rotating scaling $l_N = (F/N^3)^{1/4}$. Physically motivated scaling laws invoke angular momentum constraints and indicate the fundamental role played by rotation, which sets the scale $l_f = (F/f^3)^{1/4}$. The lateral spread of the upper-level anticyclone is constrained by rotation: for times greater than f^{-1} the anticyclone grows laterally at a rate which is essentially independent of N, and given by $l_f(ft)^{1/3}$; the ratio of the lateral scale of the anticyclone to its vertical scale (aspect ratio) is proportional to N/f. The cyclone's lateral scale is l_f, and the strong cyclonic flow scales like fl_f. An enhanced lateral mixing is suggested to occur in the cyclone along slanted angular momentum and isopycnal surfaces, which become closely aligned.

On a much longer time scale, the scaling suggests that the lateral growth of the upper level anticyclone is arrested by its interaction with the lower level cyclone; a baroclinic instability is expected to detach the anticyclone from the source after a time of order $ft \sim 100N/f$.

1. Introduction

The main contact between the hot interior of the earth and the ocean occurs at the mid-ocean ridge crest, where new crust is formed as upwelling magma solidifies. At the crest, heat is transferred to the ocean by both conduction and convection, the latter brought about by the circulation of seawater through the porous new crust. The convective or hydrothermal component is thought to amount to roughly 10^{13}W over the entire globe, emanating from thousands or perhaps millions of seafloor hot springs, called vents. The hot fluid flowing out of the vents rises in a turbulent plume and mixes with the surrounding seawater, until the mixture reaches a level where its density matches that of the water around it. At this equilibrium level it spreads out laterally, moving away from the source location and carrying with it chemical

1. Laboratoire de Physique des Océans, IFREMER, B.P. 70, 29280 Plouzané, France.
2. Center for Meteorology and Physical Oceanography, Massachusetts Institute of Technology, Cambridge, Massachusetts, 02139, U.S.A.

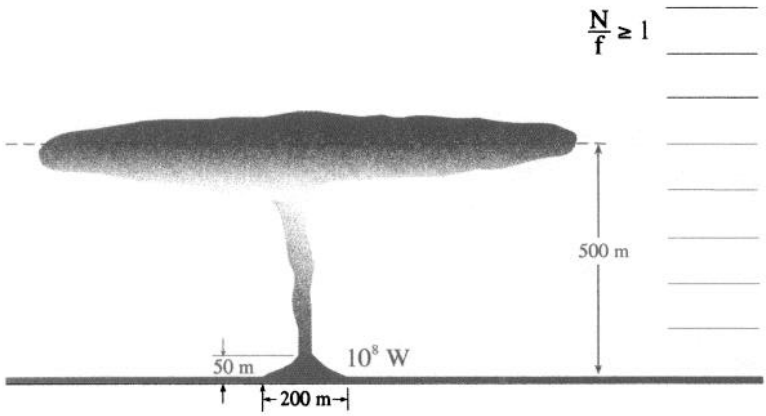

Figure 1. Schematic of hydrothermal system with a source of heat situated on a mound. A plume rises several hundred meters above the source in a narrow stem and spreads laterally at its density equilibrium level. There is a background vertical density gradient or stratification N and Earth's rotation f.

anomalies resulting from the interaction of seawater and hot rock (Fig. 1). Various tracers, including temperature-salinity anomalies, dissolved silica, manganese, and helium have been used to follow the influence of plumes at distances up to several thousands of kilometers—even across the width of the Pacific Ocean.

The seafloor vents are a substantial energy source to the deep ocean, capable of modifying the flow field as well as the property distributions at a variety of scales. The first scale of organized motion, beyond the micro- and finestructure scales associated with the turbulent mixing, is that of the rising plume. In typical deep water stratification the plume rises hundreds of meters; Lupton *et al.* (1985) observed a Pacific plume rise of nearly 200 m, while Speer and Rona (1989) found a plume rise of about 400 m above the deeper, more weakly stratified Mid-Atlantic Ridge crest. The rising plumes expand with height as water is entrained (the ratio of radius to height is roughly 0.1 [Turner, 1973, pg. 172]), but detailed comparisons of ocean observations with plume theory have not yet been possible, because of the great difficulties making observations in the deep ocean. Instead, plume theory has been used to interpret measurements, rather than using the measurements to test the application of the theory. The second scale of motion is the baroclinic vortex driven by the mass divergence in the plume (Speer, 1989). The diverging, spreading plume fluid eventually turns under the influence of rotation, creating a vortex with a typical scale of several kilometers. At much larger scales the influence of the plume can be thought of as the result of planetary wave adjustment to heating (Stommel, 1982; Joyce and Speer, 1987). Furthermore, the instability of the plume vortex (Helfrich and Battisti, 1991) or volcanic eruptions (Baker *et al.,* 1987) give rise to coherent eddies which propagate away from the source.

The distribution of conductive and hydrothermal heat flux along the crest of the mid-ocean ridge is somewhat chaotic, but larger-scale patterns exist. Variations in the heat flux are caused by variations in the thickness of the crust and by mechanical changes such as fracturing (Sclater and Francheteau, 1970; Sclater *et al.,* 1980). The structure of the underlying magmatic convection can also impress certain scales on the distribution of heat flux along the crest. This latter process could account for the occurrence of hot spots separated by about 100 km along a portion of the ridge in the North Pacific (Crane *et al.,* 1985), and may also explain part of the distribution of venting along other mid-ocean ridges. Vent systems are associated with the hot spots, consisting of both localized high-temperature chimney-like individual sources with temperatures up to more than 400°C, and low-temperature diffuse sources of typically several tens of degrees centigrade spread over larger areas. The high-temperature and low-temperature sources may produce similar total amounts of heat, but it has not yet been possible to estimate their relative contributions along a substantial portion of the mid-ocean ridge with much confidence.

The results of direct flow and temperature measurements on a few individual high temperature vents give a typical heat output of 10^6–10^7W (Converse *et al.,* 1984). Many hundreds of sources can comprise a vent system; Converse *et al.* (1984) estimate a total heat output by three vent systems at 21N on the East Pacific Rise of 2.2×10^8W, including a 35% contribution from diffuse sources. These three vent systems occupy an area roughly 1000 m × 50 m, implying an average heat flux of 4400 W m^{-2} over this limited area. Properties other than heat are transported in the vent fluid. Salt and other chemicals can affect the density of the fluid and therefore its buoyancy, rise-height, etc. An extreme example is the hot brine at the bottom of the Red Sea, which remains on the bottom because of its high salinity.

A turbulent buoyant jet is characterized (see e.g. Turner, 1986) by its initial volume flux Q [units: L^3T^{-1}], momentum source M [L^4T^{-2}], and buoyancy source F [L^4T^{-3}]. From these quantities two length scales may be constructed representing the distance to which source geometry and initial momentum influence plume evolution. A 1MW hydrothermal vent discharging at 1 m s^{-1} through a 10 cm diameter orifice has, roughly $Q = 10^{-2}$ m^3 s^{-1}, $M = 10^{-2}$ m^4 s^{-2}, and $F = 10^{-3}$ m^4 s^{-3}; at distances greater than than $l_M = M^{3/4}F^{-1/2} = 1$ m and $l_Q = Q^{3/5}F^{-1/5} = 0.3$ m the orifice geometry and momentum source are unimportant and the resulting plume may be characterized by F alone, emanating from a virtual point source about 1 m below the orifice. These distances and orifice size are all small compared to typical rise heights of tens to hundreds of meters. (Little *et al.,* 1987, provide a detailed discussion of source characteristics for a particular vent site.)

Source geometry is likely to be important even far from the source when the buoyancy b (Table 1) of the source fluid is low, since l_Q can be rewritten as $l_Q = (Q^2/\Delta b)^{1/5}$ when the velocity and density of the vent fluid are constant across the source, where Δb is the difference (anomaly) between the source buoyancy and

Table 1. Definition of basic parameters, where ρ is density, ρ_o is a constant reference density, and g is gravity.

Parameter	Symbol	Units
Coriolis parameter	f	s^{-1}
buoyancy frequency	$N = \left(-g\frac{\partial \rho}{\partial z}\right)^{1/2}$	s^{-1}
buoyancy	$b = -g\frac{(\rho - \rho_o)}{\rho_o}$	$\frac{m}{s^2}$
reduced gravity	$g' = -b$	$\frac{m}{s^2}$
thermal expansion	$\alpha = -\frac{1}{\rho}\frac{\partial \rho}{\partial T}$	$°C^{-1}$
heat flux	$\mathscr{H}$	$\frac{W}{m^2}$
buoyancy flux	$B = \frac{g\alpha\mathscr{H}}{\rho C_p}$	$\frac{m^2}{s^3}$
buoyancy source	$F = \int_{area} B\, dA$	$\frac{m^4}{s^3}$

ambient buoyancy. This may be the case for low temperature venting or diffuse sources, and a description of plume behavior in terms of a given source buoyancy anomaly or buoyancy *flux* is more appropriate as the linear dimension of the source becomes comparable to rise height. In addition, the presence of cross flow, which we ignore, due to tides, eddies, or lower frequency flow can influence the evolution and structure of plumes when it is stronger than the plume velocity scale (Middleton, 1986; Lavelle, 1994). Finally, the source is assumed to be continuous for a period long compared to either the buoyancy period (N^{-1}) or the inertial period (f^{-1}). Hydrothermal sources can remain steady for years or even centuries. A few cases of vent-extinguishing have been documented, however, and, on occasion, dramatic volcanic events rearrange the whole structure of hydrothermal circulation and heat flux on portions of the ridge.

The hydrothermal plume itself is analogous to other convective elements (Turner, 1973) which lead, for example, to the erasure of the seasonal thermocline in the ocean and penetrative deepening of the mixed layer. Plumes were a basic ingredient of the neutral convection study by Jones and Marshall (1993), who developed and applied laboratory scaling results (Fernando *et al.,* 1989; Maxworthy and Narimousa,

1994) to wintertime convection in the Mediterranean Sea. Legg and Marshall (1993) mimicked the role of stratification by adding hetons, or baroclinic vortices capable of transporting heat away from the source. Here, we are interested in how these hetons are established.

The adjustment of an initial density perturbation in the presence of rotation and stratification to a final state with balanced flow leads to a vortex shape such that the Burger number $B_g = Nh/fl \sim 1$, where h and l are vertical and horizontal scales, and N and f are stratification and rotation parameters (Table 1; Gill, 1981; McWilliams, 1988). Linear, time-independent turbulent plume and vortex models reflect this constraint on the overall size of a hydrothermal plume in terms of external scales (Speer, 1989), but questions remain about evolution and growth rates. How quickly are the different regimes established and how do they evolve to larger scales? The Burger number characterizes the stability boundaries of vortices as well; flow with a Burger number much greater or less than unity tends to be unstable (e.g. McWilliams *et al.,* 1986). The laboratory study of Helfrich and Battisti (1991) provides a helpful background to a study of the evolution of the hydrothermal vortex. They supplied dense water to a rotating tank in which a stable stratification was established. The dense water (representing an upside-down hydrothermal source) entrained ambient fluid and sank to its equilibrium level, where it spread horizontally. A baroclinic vortex was created which grew in size but remained attached to the source until it became baroclinically unstable and moved away.

Our goal in this investigation of hydrothermal convection is to present consistent and unified scaling laws which describe the evolution of the system from a rising plume to a rotating vortex to detached hydrothermal eddies, and to support these through numerical experiment. We attempt to analyze how a system with rotation and stratification responds to a localized boundary heat source, by using approximate bulk mass and buoyancy conservation to relate the various plume scales to the external parameters of the system. Without stratification, the key length scale in the convecting system formed by combining the forcing F with rotation is $l_f = (F/f^3)^{1/4}$. the length scale l_f is known from theoretical studies of convection (Stone, 1968), from laboratory studies of mixed layer deepening with rotation in a nonstratified basic state (Hopfinger *et al.,* 1982; Fernando *et al.,* 1989; Maxworthy and Narimousa, 1994) and from numerical simulations of ocean convection (Jones and Marshall, 1993; Marshall *et al.,* 1994). For hydrothermal vents, $F \sim 10^{-2}\ \mathrm{m^4\ s^{-3}}$, and $f \sim 10^{-4}\ \mathrm{s^{-1}}$, giving $l_f \sim 300$ m. The ratio l_f/H, where H is the distance to the nearest boundary or sea surface, is presumed here to be small, so that rotation can exert a controlling influence. Without rotation, on the other hand, the key length scale is $l_N = (F/N^3)^{1/4}$. The ratio of l_N to l_f is $(f/N)^{3/4}$, exposing the parameter f/N connecting the two systems. Away from mixed layers in the ocean f/N is usually small, ranging from roughly 1/10 (deep water) to 1/100 (thermocline). Scaling arguments presented

below include both stratification and rotation and show that the rotation scale l_f still plays a fundamental role even in the presence of stratification.

Numerical simulations which, in principle, include all of the physics are used to test the scaling arguments. The numerical model solves the incompressible Navier-Stokes equations at high spatial resolution. Our approach is similar to that of a laboratory experiment; scales from the simulation are used as a reference against which scaling laws drawn from simple physical arguments can be compared and evaluated. First, in Section 2, we describe the basic structure of evolving hydrothermal plumes as seen in our numerical model. This provides the context for the development of scaling laws, Section 3, which are then assessed in the light of numerical experiments in Section 4. Conclusions follow in Section 5.

2. Hydrothermal experiments with a convection model

The non-hydrostatic Navier Stokes convection model described in Brugge *et al.* (1991) was employed to study the underlying fluid dynamics that control the evolution of a hydrothermal plume in a stratified, rotating ocean. Details of the model and its numerical implementation can be found in the Appendix. Our strategy was to adopt the simplest and most straightforward approach possible in these experiments. The model was configured in a doubly-periodic, 15 km domain in a 2 km deep ocean, with a uniform grid-spacing of 50 m both in the horizontal and vertical (Fig. 2). Sub-grid-scale processes were parameterized using isotropic laplacian 'eddy' diffusion of heat and momentum with constant coefficients. Eddy diffusivities were reduced to the absolute minimum required to obtain smooth fields on the grid-scale of the model; a choice of $\nu = \kappa = 0.1\ \mathrm{m^2\,s^{-1}}$ was used in all the experiments presented here, implying a diffusive time-scale over one grid-cell of the model of 7 hrs, much longer than the advective time-scale of 0.1–1 hr.

A linearized equation of state was employed of the form

$$\rho = \rho_o(1 - \alpha T)$$

where ρ_o is a constant reference density and $\alpha = 2.1 \times 10^{-4}\ ^\circ\mathrm{C}^{-1}$ the coefficient of thermal expansion of water. A resting, stably-stratified fluid characterized by a linear temperature profile implying buoyancy frequency, N, with

$$N^2 = g\alpha \frac{\partial T}{\partial z},$$

was subject to a buoyancy forcing at the bottom. A tracer field was injected into the fluid over the heating region, to mark the fluid and aid flow visualization.

The experiments carried out are summarized in Table 2. In all cases F, ν, κ, were kept fixed but the ambient stratification N and rotation rate f were varied. The buoyancy forcing was interpreted and applied as an increment of temperature over grid boxes adjacent to the bottom of the model, with strength $F_o = 2.3 \times 10^{-2}\ \mathrm{m^4\,s^{-3}}$

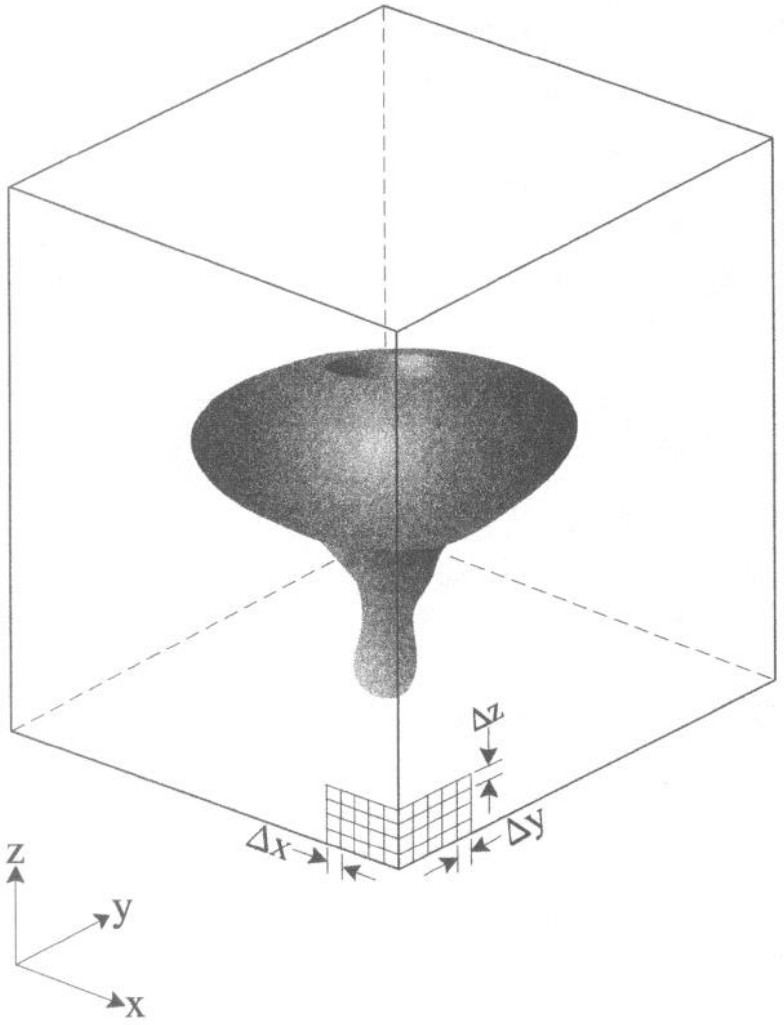

Figure 2. Numerical model geometry for hydrothermal plume simulation. Grid resolution $\Delta x = \Delta y = \Delta z = 50$ m. Within the model frame, a surface of constant tracer concentration is displayed, showing the narrow stem below the expanding equilibrium level lens (run 10).

(or about 92 MW) over an area 100 m × 100 m in the center of the domain. This corresponds to a heat flux of 9200 Wm^{-2} over the area 10^4 m^2, which is a plausible source for a hydrothermal system. We proceed to describe our reference experiment (run 10), for which $N = 4 \times 10^{-4}$ s^{-1} ($N/f = 4$), to provide a description of the nature of the numerical solutions obtained. Quantitative evaluations of the experiments are presented in Section 4, in light of the scaling ideas outlined in Section 3.

In response to the warming a buoyant plume rises and settles at its neutrally buoyant level Z_{obs} (we denote the observed height in the model runs by Z_{obs}, and the

Table 2. Model runs.

Run	$f \times 10^4\ s^{-1}$	$N \times 10^4\ s^{-1}$	Z_N m	Symbol
1–5	test			
6	1	2	871	+
7	0	2	871	dotted
8	1	1.5	1080	o
9	test			
10	1	4	517	×
11	0	1.5	1080	
12	0	4	517	
13	1	3	639	*
14	1	5	436	solid

predicted height from plume theory as Z_N). As it rises it carries with it dye which marks fluid that has been convectively modified. Figure 3 shows a vertical section through the dye at 2 days. There is a narrow stem topped by a bulbous head which grows in size as fluid, convectively modified in the stem, flows out at the neutrally buoyant level, near 350 m height.[3] An examination of individual particle trajectories in the simulation showed particles spiralling cyclonically inwards at the base toward

3. The absence of salinity implies that the plume fluid spreading at its equilibrium level has the same temperature as the surroundings. Speer and Rona (1989) examined equilibrium level anomaly dependence on salinity.

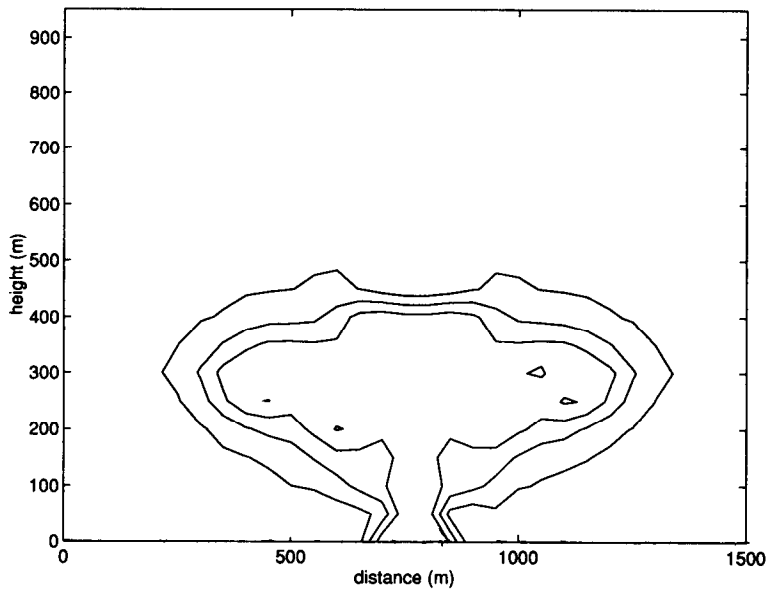

Figure 3. Vertical section of tracer after 2 days (run 10). Extreme values near source excluded, contours interval 10%, from 10% (outermost) to 40% concentration.

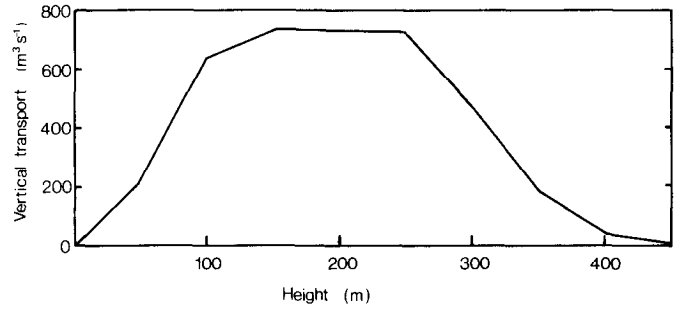

Figure 4. Vertical mass transport ($m^3\ s^{-1}$) versus height in the rising plume (stem), at 2 days (run 10).

the stem, rising up in it, exiting, and 'unwinding' in the anticyclonic head. A surface of constant dye intensity in three-dimensions vividly outlines the structure of the baroclinic vortex, with a narrow stem and broad bulb on top (Fig. 2).

A basic characteristic of the rising plume is the enhancement of its vertical mass transport as fluid is entrained. An instantaneous view of transport two days after switching on the heat source shows the transport increasing up to about half way to the top of the plume (Fig. 4). The magnitude of the transport is also in broad agreement with scaling ideas presented in Section 3. Detrainment is centered at the spreading level of ~ 350 m, and the vertical extent of the detrainment clearly defines the thickness of the spreading layer at its origin.

Of special interest is the horizontal flow spun up by the entrainment-detrainment structure. Divergent flow drives an anticyclone at 350 m and 400 m height with speeds of typically 0.5 cm s^{-1} (Figs. 5 and 6), while convergence at lower levels generates a strong cyclone where speeds in excess of 10 cm s^{-1} can be found. We observe that the Rossby number, u/fl, is small in the anticyclone, but of order unity in the cyclone. In the lower part of the anticyclone the vorticity advection term $w\zeta_z$ is the same order as ζ_t, and the core of the vortex is actually cyclonic, because of a strong vertical advection of vorticity.

The distinction between a heat-source driven cyclone and mass-source driven anticyclone is a fundamental theme of this study. Warm temperature anomalies are generated directly above the heat source and actively drive vertical and horizontal motion. The passive nature of temperature, however, in the mass-driven anticyclone above is evident on a horizontal, plane view in the upper part of the anticyclone (Fig. 7). The temperature anomaly spirals out from the center a distance of several kilometers along a branch, over a time period of 50 days. The inferred velocity of a few millimeters per second is indeed consistent with the strength of the horizontal flow, supporting an advective interpretation of the feature.

At 450 m, a small-scale cyclonic core gives the anticyclone a more complicated horizontal structure, but at greater distances from the axis the vortex is not far from

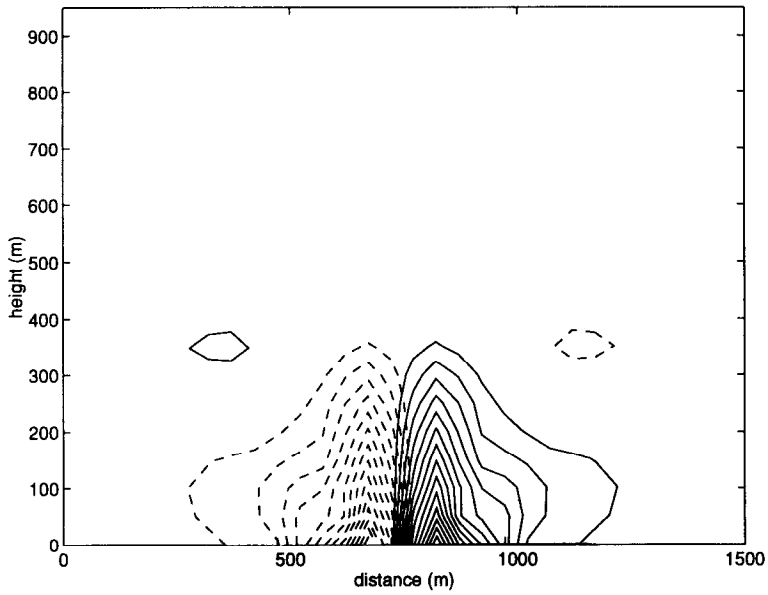

Figure 5. Isopleths of azimuthal flow (day 2, run 10). Circulation is cyclonic below about 300 m (maximum 0.12 m s^{-1}) and anticyclonic above (maximum 0.01 m s^{-1}). Contour interval 7 mm s^{-1}; overlap marks location of rising plume.

solid-body rotation (Fig. 8). Beyond a radius of 400 m, which is about 20% of NZ_N/f, where Z_N is the rise-height from non-rotating plume theory, the flow decays to zero. Taking the overall structure of the core to be solid-body rotation with $V = fr/2$, the vorticity $\zeta = f$. This result is consistent with Hedstrom and Armi (1988), whose laboratory work suggests that $\zeta = f$ in an anticyclonic lens generated by a mass source. For long times the Rossby number does not remain constant, however, but rather decreases as the plume expands and slows.

The process by which azimuthal currents are generated is revealed more clearly by a study of the geometry of the angular momentum surfaces. For axisymmetric flow the angular momentum at a distance r from the origin is

$$m = \tfrac{1}{2}fr^2 + rv.$$

Surfaces of constant m are thus initially cylinders surrounding the source at the origin. In the limit of zero viscosity and perfect symmetry the angular momentum is conserved, i.e., the volume within and between each cylinder is conserved. This was tested in our numerical experiment; the volume was found to be conserved to a few percent, except very near the source (within a few hundred meters) where the balance was off by as much as 10%.

The contraction and expansion of the m-surface provides a useful measure of initial particle displacement. Using the maximum outward displacement for the

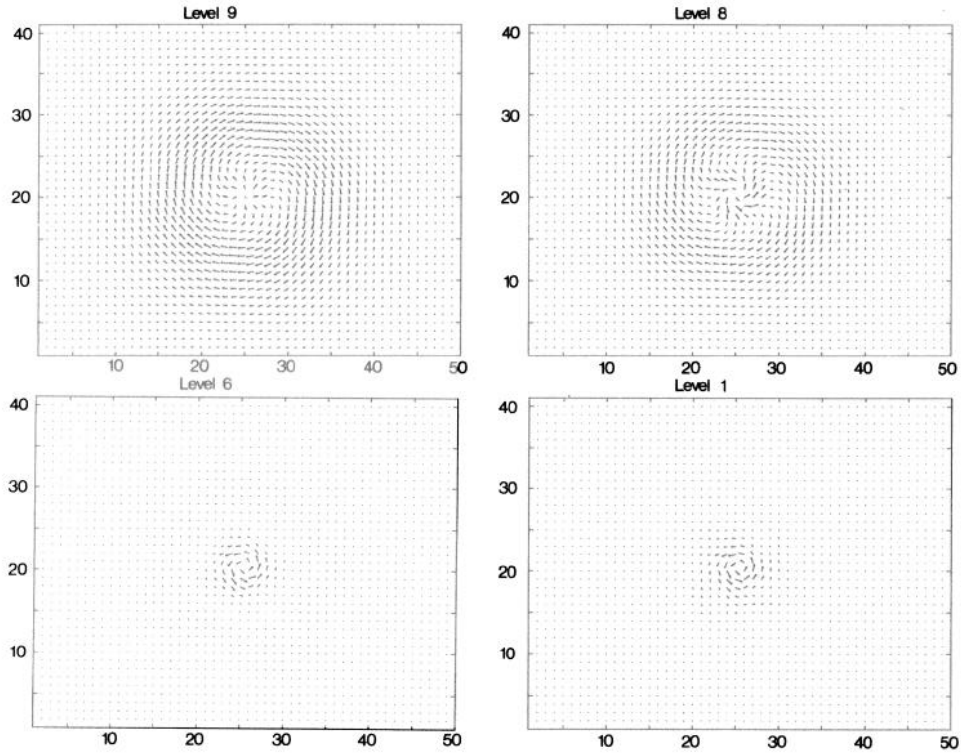

Figure 6. Plan view of horizontal velocity field (run 10, day 2), at 4 levels: 1 (50 m, max. 12 cm s^{-1}), 6 (300 m, max. 3.5 cm s^{-1}), 8 (400 m max. 1.1 cm s^{-1}), and 9 (450 m, max. 0.7 cm s^{-1}). Axes are gridpoints over a subset of the model domain, centered on the source.

anticyclone and the maximum inward displacement for the cyclone, the velocity scale in both vortices obeys the relation:

$$V = f\,\delta r,$$

where δr is the displacement of the surface from its reference radius. Figure 9 shows a section of m and ρ at ten days through the middle of the hydrothermal plume. The stratification in the vertical due to ρ, and in the horizontal due to m, is clearly evident. Velocity (u, w) in this plane is superimposed. The rising plume appears as a jet in the middle, which at higher levels has spread out to include cooler water on either side of the warm central core. At large distances isopycnals and angular momentum surfaces are perpendicular; near the plume the isopycnals dip and m-cylinders deform to the extent that these two fields become parallel or cross. For two-dimensional symmetric flow this implies that potential vorticity is close to zero. We speculate that symmetric instability in this situation (see, e.g., Thorpe and Rotunno, 1989) generates small-scale eddies around the edge of the plume. Rather than interacting in a horizontal

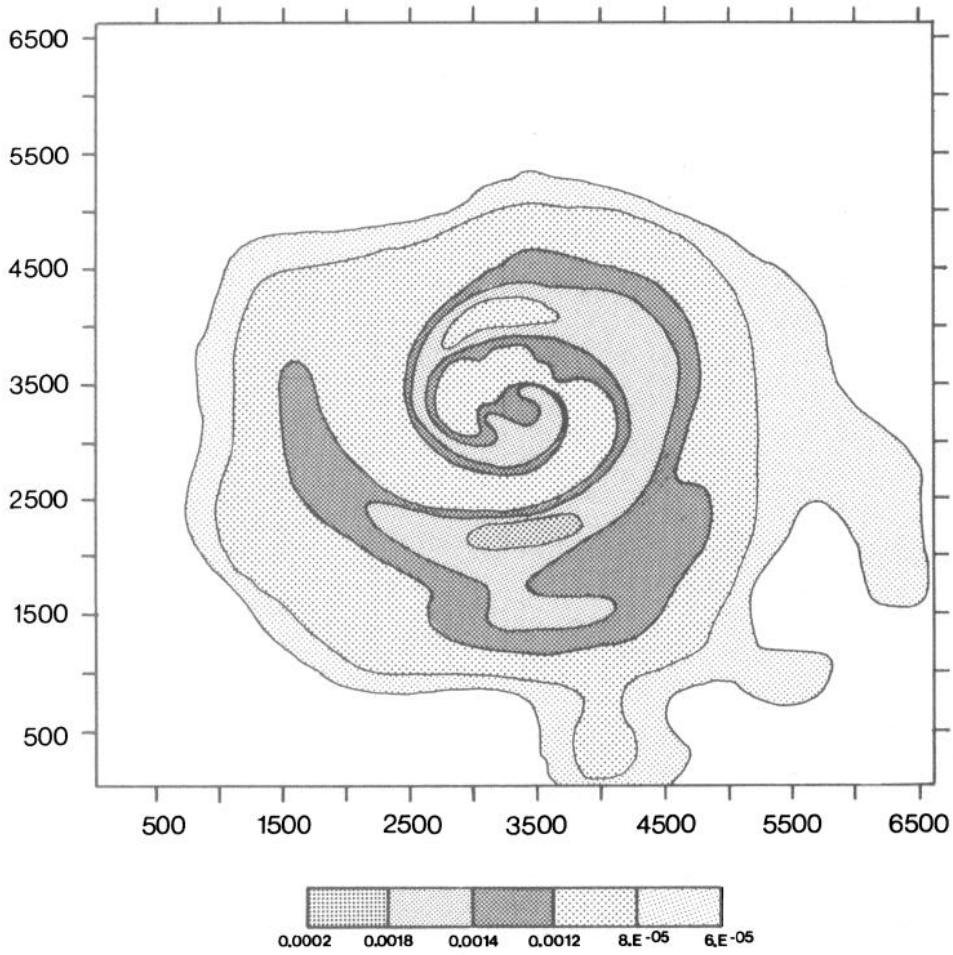

Figure 7. Temperature anomaly (°C) at 700 m height (day 50, run 14). Horizontal distance in meters. The anomaly spirals out from the center in the anticyclonic flow at this level above Z_N.

plane, plume fluid and ambient fluid parcels appear to circulate and mix intensively in slanted layers bounded by parallel m and ρ surfaces.

The integration presented in Figures 3 to 9 was continued out to sixty days but, somewhat perplexingly, did not show any evidence of baroclinic instability. We return to this aspect in Section 3 and again in Section 4.

3. Physical balances and scaling laws

Consider a source of buoyancy of strength F switched on at $t = 0$. As observed in our numerical experiments, buoyant fluid will rise, entrain surrounding fluid, and

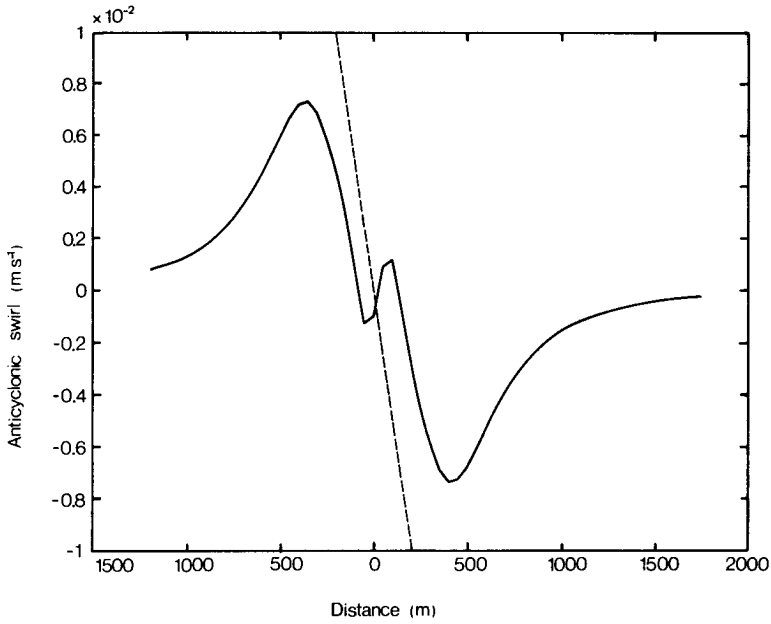

Figure 8. Plot of anticyclonic flow at 450 m height (day 2, run 10). Dashed line is solid-body flow $fr/2$.

settle at its (observed) neutrally buoyant level Z_{obs}. Below this level, the fluid drawn in will eventually feel the presence of rotation and begin to swirl cyclonically; at the spreading level, fluid will spiral out in the anticyclonically spinning head of the vortex. We suppose that this upper part of the vortex is characterized by a lateral dimension l and a thickness scale h centered on the spreading level. All scales are a function of time.

We now attempt to understand the dependence of the scales Z_{obs}, l, h, and the associated buoyancy and velocity scales on the external parameters F, N, f, and t. It is assumed that stratification effects occur first, i.e., that $N/f > 1$.

a. Time $t \ll N^{-1}$

At these short times the only two important physical variables are the source F (units $m^4\ s^{-3}$) and time t. Constructing length, velocity, and buoyancy scales from F and t yield

$$z = (Ft^3)^{1/4}$$
$$w = \left(\frac{F}{t}\right)^{1/4} \qquad (1)$$
$$g' = \left(\frac{F}{t^5}\right)^{1/4}.$$

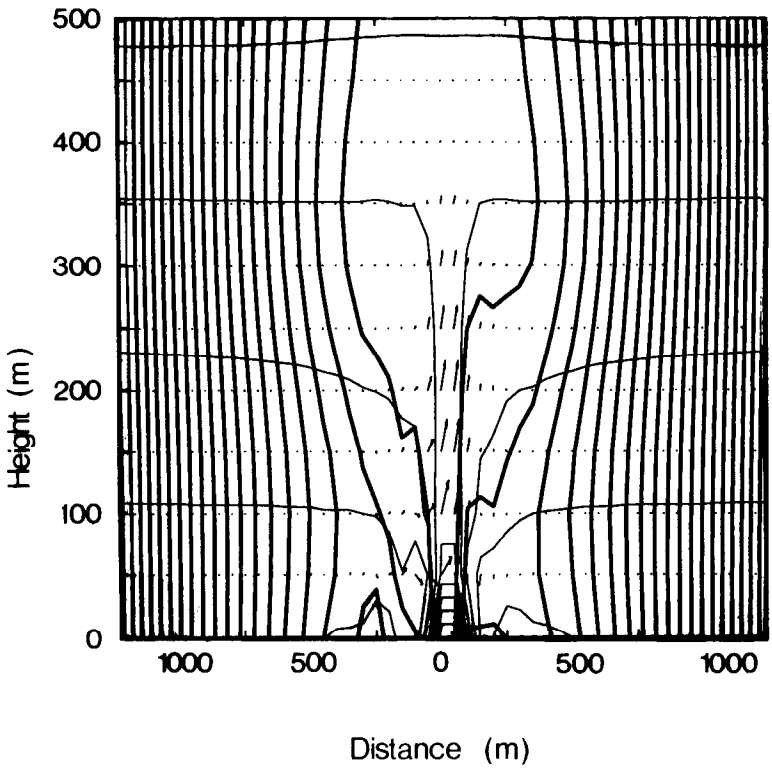

Figure 9. Profile of temperature (light) and angular momentum (heavy), with velocity superimposed (max. vertical velocity 4 cm s^{-1}; day 2, run 10). In the cyclone, temperature and angular momentum surfaces tend to become parallel.

In neutral conditions (no stratification) the entrained water always has the same density, and while the average buoyancy of the plume at any level decreases, the total vertical buoyancy transport must remain constant. The net buoyancy force is always positive, and the plume gathers momentum not by increasing its speed but rather its area. The scales for the cross-sectional area of the plume A, vertical velocity w, and buoyancy g' can be expressed in terms of the height $z = wt$ above the source; eliminating t in (1) in favor of z gives the traditional plume scales:

$$\begin{aligned} A &= z^2 \\ w &= (F/z)^{1/3} \\ g' &= b = (F^2/z^5)^{1/3}. \end{aligned} \tag{2}$$

Turner (1973) provides a discussion of similarity solutions based on such scaling.

With nothing to balance the upward buoyancy force the plume would continue rising until it ran into a boundary. However, the presence of stratification sets a time scale N^{-1} at which the vertical penetration of the plume is restrained as the buoyancy force diminishes. In the absence of stratification, the plume's behavior changes only

as the time scale approaches that of rotation f^{-1}, by which time significant horizontal motion has been generated.

b. Time $t \rightarrow N^{-1}$: Rising plume

The stratification time scale or buoyancy period N^{-1} (up to more than 1 hr in deep water) and the source strength F together set length, buoyancy, and velocity scales in the rising plume. These are obtained by substituting $t = N^{-1}$ in (1):

$$\begin{aligned} h_N &= (F/N^3)^{1/4} \\ g'_N &= (FN^5)^{1/4} \\ u_N &= (FN)^{1/4}. \end{aligned} \tag{3}$$

These scales form the basis for plume models which have an application to a wide variety of natural phenomena (see Turner, 1986, for a review). The vertical penetration scale Z_N has been calibrated in the laboratory and the field over a large range of F and N and consistently shows that plumes penetrate a distance close to

$$Z_N = 3.76 h_N \tag{4}$$

where they spread horizontally at their equilibrium density level. The constant of proportionality in (4) has been derived empirically by fitting to numerous laboratory and field experiments of buoyant plumes (Turner, 1986).

c. Time $N^{-1} < t < f^{-1}$: The baroclinic vortex

As time progresses beyond N^{-1} the plume, having reached its equilibrium level, begins to fill the surrounding layer with plume of density $\rho(z = Z_N)$.

The existence of an equilibrium level, a consequence of the stratification, effectively isolates the part of the water column above this level from the buoyancy source. That is, since the total vertical buoyancy transport across this level is zero, the region above does not 'see' the heat source directly. Instead, the region above sees only a source of mass at the equilibrium density. Thus we divide the scaling problem into two distinct parts. First, there is the anticyclonic, upper mass source regime, in which an inflating blob of plume fluid spreads horizontally and begins to spin anticyclonically as it tries to conserve angular momentum. Second, there is the cyclonic, lower buoyancy source regime, over which the buoyancy source F converges and heats the surroundings, thereby displacing isopycnals downward. Again, in an attempt to conserve angular momentum, water flowing toward the rising plume as a result of entrainment eventually turns and spins up the cyclonic flow.

i. The anticyclone. Conservation of mass for the lens of plume fluid growing above the equilibrium level requires:

$$l^2 h = W Z_N^2 t \tag{5}$$

or

$$l^2h = NZ_N^3 t = \left(\frac{F^3}{N^5}\right)^{1/4} t, \tag{6}$$

where l, h are lens dimensions, and $WZ_N^2 = NZ_N^3$ is the lens mass source or mass transport scale at the top of the rising plume. Empirically, we observe that the plume diameter is roughly one-tenth the height, giving an area smaller by the factor 0.01, and hence mass source closer to 0.01 WZ_N^2. According to simple adjustment theory, the mass anomaly created by the source spreads radially as a front propagating at the gravity wave speed:

$$l = \sqrt{g'ht} = Nht, \tag{7}$$

where we have supposed that this speed is Nh. A balance between kinetic and potential energy gives the final speed u if all the energy is converted:

$$\tfrac{1}{2}\rho u^2 = g\Delta\rho h. \tag{8}$$

Then since:

$$\frac{g\Delta\rho h}{\rho_o} = \frac{g}{\rho_o}\int_o^h z\frac{\partial\rho}{\partial z}dz = \frac{N^2h^2}{2}, \tag{9}$$

we see that $u = Nh$, as assumed above in (7).

Combining expressions for the mass conservation (6) and expansion rate (7), we obtain

$$h = Z_N(Nt)^{-1/3}, \tag{10}$$

$$l = Z_N(Nt)^{2/3}. \tag{11}$$

The volume of plume fluid expands very quickly at first, thinning in the middle. The aspect ratio $h/l = (Nt)^{-1}$ decreases with time, beginning at $t = N^{-1}$ with a value of unity as the blob is formed. As $t \to f^{-1}$ the aspect ratio decreases to f/N as the mass begins to sense the constraint imposed by rotation, limiting displacements to a local deformation radius. This behavior qualitatively explains the initial rapidly decreasing aspect ratio observed by Helfrich and Battisti (1991) in laboratory experiments.

ii. The cyclone. The region below the equilibrium level is forced directly by the buoyancy source. Conservation of buoyancy in this region implies:

$$\begin{aligned} l_c^2 h_c g_c' &= Ft \\ l_c &= Nh_c t \end{aligned} \tag{12}$$

where l_c and h_c are horizontal and vertical dimensions for the cyclone and g' is the reduced gravity. The vertical dimension of the cyclone is also a measure of the height

at which cyclonic vorticity changes to anticyclonic vorticity, and hence is a scale for the rise height Z_{obs}. Again, the mass or isopycnal disturbance propagates with speed Nh_c, so $l_c = Nh_c t$. To find the dependence of these scales on basic parameters, write

$$\begin{aligned} h_c &= L_N \phi(Nt) \\ g' &= g_N \phi(Nt) \end{aligned} \tag{13}$$

where $\phi(Nt)$ is some function of Nt to be determined. The above form is chosen so that the scales evolve from time $t = N^{-1}$ in the same manner. Substituting into (12) and solving we find that $\phi = (Nt)^{-1/4}$, and so

$$\begin{aligned} g'_c &= (FN^5)^{1/4}(Nt)^{-1/4} \\ h_c &= (F/N^3)^{1/4}(Nt)^{-1/4} \\ l_c &= (F/N^3)^{1/4}(Nt)^{3/4} = (Ft^3)^{1/4}. \end{aligned} \tag{14}$$

d. Time $t = f^{-1}$

In the anticyclone, as $t \to f^{-1}$ the lens of plume fluid has the dimensions, replacing t by f^{-1} in (10) and (11), of

$$h = Z_N \left(\frac{f}{N}\right)^{1/3}; \qquad l = Z_N \left(\frac{N}{f}\right)^{2/3}. \tag{15}$$

For later comparison to numerical solutions (Section 4) the N dependence is of particular interest. Thickness h varies like $N^{-13/12}$, or very nearly N^{-1}, while $l \sim N^{-1/12}$ is essentially independent of N.

In the cyclone, as $t \to f^{-1}$, the following scales emerge:

$$\begin{aligned} l_c &= l_f = (F/f^3)^{1/4} \\ h_c &= \frac{f}{N} l_f \\ g'_c &= N f l_f \\ v_c &= f l_f. \end{aligned} \tag{16}$$

The velocity scale may be obtained from the thermal wind relation $v_c = g'_c/N$, or $v_c = fl_f = (Ff)^{1/4}$.

We see that as time increases from the buoyancy period to the rotation period, the scales of the system expand from those associated with the tall, thin inner turbulent plume to those of the cyclone. The reduced gravity now depends on f because the larger scale isopycnal deformation surrounding the plume is associated with thermal wind. Remarkably, even in the presence of stratification with its own time scale N^{-1}, the length scale l_f reappears as a fundamental plume scale independent of N.

In the neutral convection problem l_f was a vertical penetration scale for a density anomaly into a neutral environment. It can also set the lateral scale of convective

plumes (Marshall *et al.*, 1994; Helfrich, 1994). Here, with stratification, it appears from conservation principles as a horizontal or, more precisely, a slanted convection displacement scale on the sloping isopycnals of the cyclone (of slope $h_c/l_f = f/N$).

e. Time $t > f^{-1}$

At times greater than f^{-1} the mass source continues to pump fluid into the anticyclone. We assume that the evolution consists of continual adjustment, such that the Burger number (Nh/fl) remains of order unity. With the aspect ratio now constrained, conservation of mass implies

$$l^3 \frac{f}{N} = NZ_N^3 t, \tag{17}$$

so that

$$l = Z_N \left(\frac{N}{f}\right)^{1/3} (Nt)^{1/3} = l_f \left(\frac{f}{N}\right)^{1/12} (ft)^{1/3} \tag{18}$$

$$h = Z_N \left(\frac{f}{N}\right)^{2/3} (Nt)^{1/3} = l_f \left(\frac{f}{N}\right)^{13/12} (ft)^{1/3}. \tag{19}$$

Now both dimensions grow with time like $(ft)^{1/3}$. The N dependence is the same as in (15): l is nearly independent of N and h is essentially inversely proportional to N.

For times longer than the rotation period, the steady buoyancy input continues to heat the cyclone as well as supply mass to the anticyclone. Again assuming that the aspect ratio remains equal to f/N, and using conservation of buoyancy implies:

$$\begin{aligned} l_c &= l_f (ft)^{1/4} \\ h_c &= \frac{f l_c}{N} \\ g_c' &= N f l_f (ft)^{1/4}. \end{aligned} \tag{20}$$

Note that the scale for the rise height h_c can be written as $h_c = Z_N (f/N)^{1/4} (ft)^{1/4}$. Thus the rise height scaled by Z_N has a weak dependence on f and N, and grows with time like $t^{1/4}$.

f. Anticyclonic velocity scale

Much of the previous scaling pertains to tracer quantities because it invoked integral balances of mass and buoyancy. A distinction needs to be made in principle between the dimensions of the anticyclonic lens (h, l) represented by the tracer distribution and the size of the horizontal and vertical displacements of material surfaces and fluid parcels. We now consider the velocity scales associated with the displacement of angular momentum surfaces (Δr) and with density surfaces (Δz) (Fig. 10) through the thermal wind and angular momentum relations.

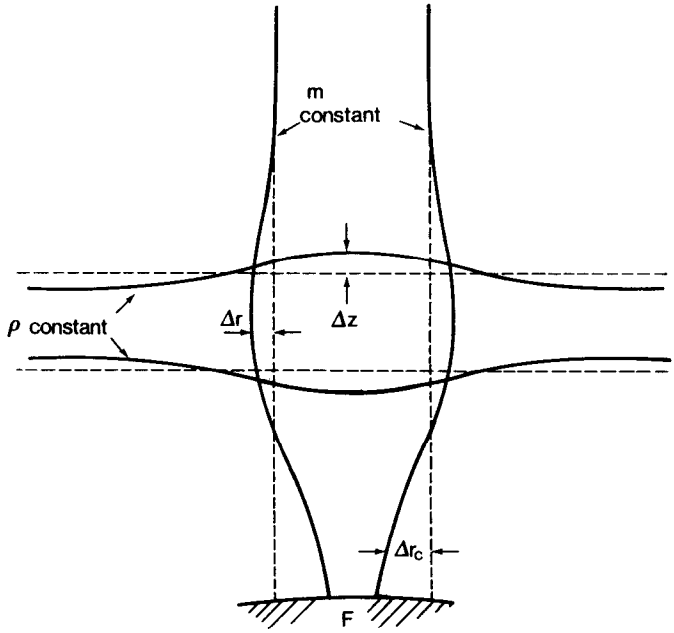

Figure 10. Displacement length scales.

We observe that the lateral displacement scale of the angular momentum surface in the anticyclone is less than that of the tracer field. Moreover, the displacement scale is set after roughly one day and remains relatively constant thereafter. If the displacement scale were as large as the tracer scale, then very high velocities would eventually occur, and the Rossby number $V/fl = f\Delta r/fl$ would be identically one for all time, whereas it is observed to be much smaller than one. A related observation is that the location of maximum swirl velocity remains almost fixed after one rotation period, though fluid parcels spiral outward with the tracer (Fig. 7).

The lateral scale of the tracer l and the lateral displacement of the angular momentum surfaces can differ from one another by some function of the fundamental parameter f/N. Suppose provisionally (excluding time dependence) that

$$\Delta r = \left(\frac{f}{N}\right) l. \tag{21}$$

The thermal wind and angular momentum relations are:

$$V_{ther} = \frac{g'\Delta z}{f\Delta r}, \tag{22}$$

$$V_{ang} = f\Delta r, \tag{23}$$

assuming that Δr is the scale over which the vertical displacement of the isopycnal Δz decays to zero. If (22) and (23) are to give the same velocity scale, then $g' =$

$(f\Delta r)^2/\Delta z = N^2\Delta z$ using the aspect ratio $\Delta z/\Delta r = f/N$. Thus the appropriate buoyancy scale g' for the anticyclone is that set up dynamically by the thermal wind, $\Delta z N^2$. [Note that the thickness $h \sim l(f/N)$ is greater than Δz by the factor N/f because it represents a bulk mass balance rather than a dynamical constraint.]

Empirical results from the numerical simulations (Section 4) are indeed consistent with these ideas; an analysis of several numerical solutions suggests that the following N-dependencies hold:

$$\begin{aligned} \frac{h}{l} &\sim \frac{f}{N}; \qquad V \sim N^{-1} \\ h &\sim N^{-1}; \qquad \Delta r \sim N^{-1}. \end{aligned} \tag{24}$$

With the above scales (22–23), V has the observed (24) N-dependent scale $N\Delta z$ rather than Nh, which is only weakly dependent on N.

The relation

$$\frac{\Delta z}{h} = \frac{\Delta r}{l} = \frac{f}{N} \tag{25}$$

suggests that in the limit of low N/f the displacements are relatively large. In the opposite high stratification or low rotation limit (for fixed F) the displacements are tiny compared to tracer scales. The Rossby number measured by displacements is $R_o = u/f\Delta r = f\Delta r/f\Delta r = 1$, but measured over the lens by the tracer scale it is $f\Delta r/fl = \Delta r/l = f/N$.

g. Instability time scale

The plume would continue to grow forever were it not for the existence of a dynamical instability which breaks it apart. Baroclinic instability theory predicts that vortices with a radius greater than the deformation radius should be unstable to perturbations of the swirl velocity (Pedlosky, 1985; Helfrich and Send, 1988), such that they break into two separate vortices.

Setting the radius of the anticyclonically spinning volume of plume fluid (18) to the deformation radius gives

$$Z_N \left(\frac{N}{f}\right)^{2/3} (ft)^{1/3} = \frac{N}{f} Z_N \tag{26}$$

or

$$ft = 100 \frac{N}{f}, \tag{27}$$

where a coefficient of 100 is suggested by the empirical factor relating vertical transport to its scale (see the discussion following (6)). This is the time scale it takes

Table 3. Scaling summary.

Rising plume	
rise height	$l = h_N = (F/N^3)^{1/4}$
buoyancy	$g' = g_N = (FN^5)^{1/4}$
velocity	$u = u_N = (FN)^{1/4}$

Anticyclone			
	$N^{-1} \le t \le f^{-1}$	$t \ge f^{-1}$	$t \simeq 100 \frac{N}{f} f^{-1}$
diameter	$l = Z_N(Nt)^{2/3}$	$(f/N)^{1/12} l_f (ft)^{1/3}$	$Z_N N/f$
thickness	$h = Z_n(Nt)^{-2/3}$	$(f/N)^{13/12} l_f (ft)^{1/3}$	Z_N
buoyancy	$g' = N^2 h$	$N^2 \Delta z$	$N f Z_N$

Cyclone			
	$N^{-1} \le t \le f^{-1}$	$t \ge f^{-1}$	$t \simeq 100 \frac{N}{f} f^{-1}$
diameter	$l_c = (Ft^3)^{1/4}$	$l_f (ft)^{1/4}$	$Z_N N/f$
stem height	$h_c = Z_N(Nt)^{-1/4}$	$l_f (f/N)(ft)^{1/4}$	Z_N
buoyancy	$g' = g_N(Nt)^{-1/4}$	$N f l_f (ft)^{1/4}$	g_N

the rising plume to transport vertically an amount of mass equal to that in a volume within a deformation radius of the source, and is the time at which the plume will become baroclinically unstable. By this time, the buoyancy g' in the cyclone (20) has strengthened up to its original nonrotating scale $(F/N^5)^{1/4}$ owing to the continued heating.

A summary of the scaling is presented in Table 3, and Figure 11.

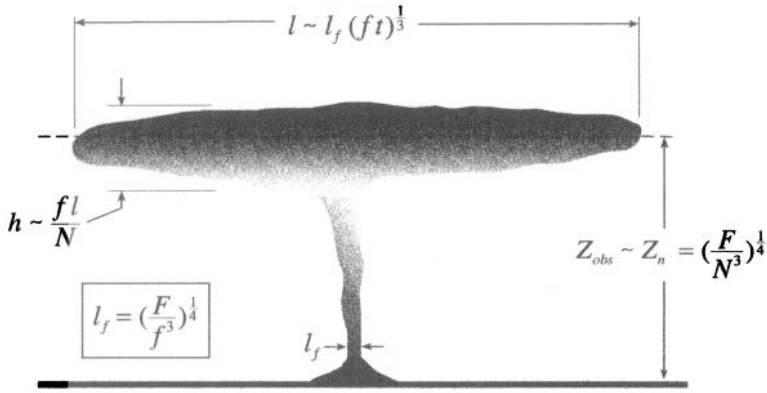

Figure 11. Rotating plume length scales.

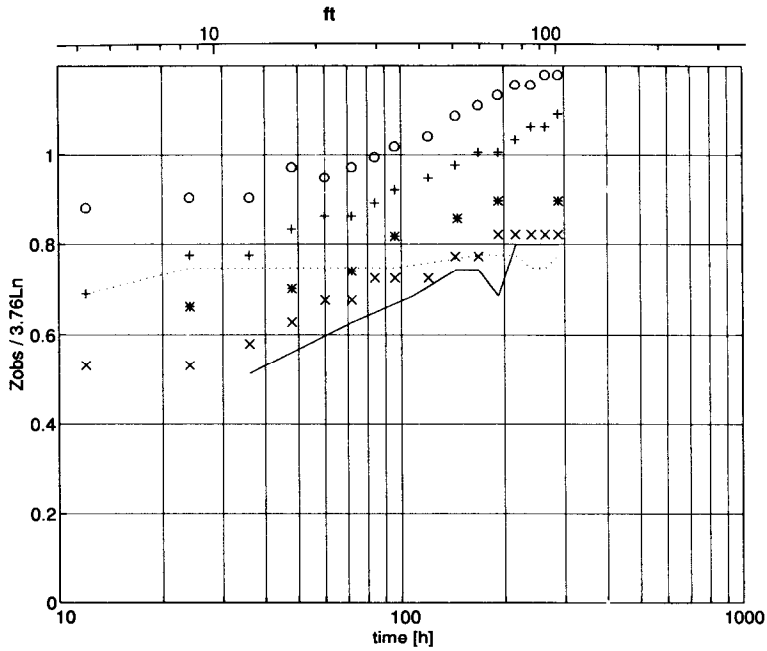

Figure 12. Penetration height scaled by Z_N versus time (hours and nondimensionalized by $f = 10^{-4}\ s^{-1}$). Run 8 (○), run 6 (+), run 13 (*), run 10 (×), run 14 (solid), run 7 (dotted); see Table 2.

4. Quantitative interpretation of hydrothermal simulations

a. Rising plume

Helfrich and Battisti (1991) noted a basic agreement between their laboratory measure of observed spreading height and that predicted by the plume scaling Z_N (calibrated empirically), but with significant scatter. In the numerical simulations too, we find a consistent qualitative agreement. The mean value of the ratio of the initial tracer spreading level to Z_N (as given by (4)) at day 1 was 0.70 ± 0.13, using six runs.

Plots of tracer spreading level versus time, normalized by Z_N (Eqs. 3 and 4), soon separate into rotating and nonrotating groups (Fig. 12; dotted line marks nonrotating run). After a rise time of order N^{-1} the nonrotating plume remained at its initial equilibrium level. (In the low-N runs this time is nearly the same as f^{-1}, and so they are still adjusting after one day.) In the presence of rotation, however, the plumes continued to evolve at long times, with a dependence broadly consistent with the $t^{1/4}$ behavior expected from consideration of the buoyancy budget of the cyclonic stem (20). Helfrich and Battisti (1991) observed a superpenetration of the plume, that is, an increasing penetration with time from an initial height close to Z_N, but they did not attempt to quantify the time dependence. They attributed this growth to a

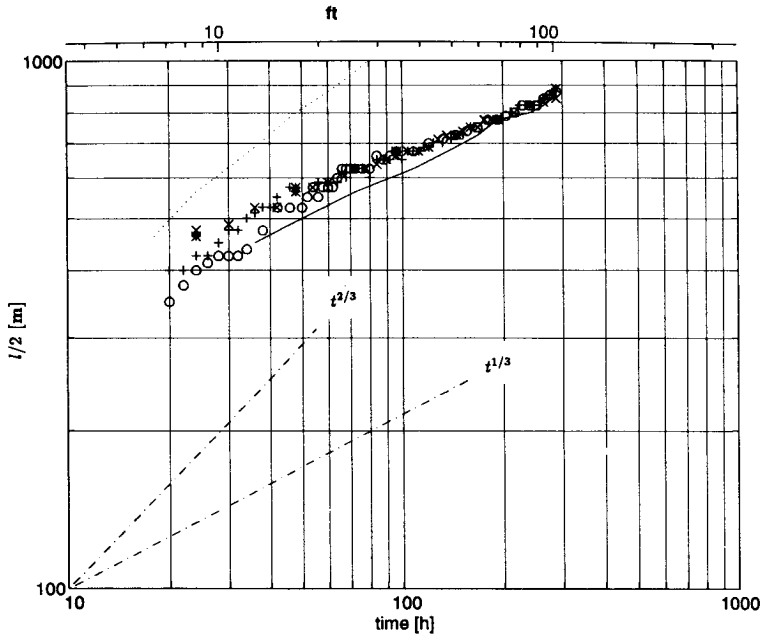

Figure 13. Radius of anticyclonic lens versus time. A $t^{2/3}$ and $t^{1/3}$ dependence is shown for reference [see caption to Fig. 1 and Table 2].

reduced stability surrounding the rising plume as fluid is drawn down from the spreading layer because of rotational effects (see e.g., Speer, 1989). A gentle rising (and weak N-dependence) of the neutrally buoyant level with time is predicted by the scaling h_c (20), owing to the evolution of the buoyancy and therefore stratification in the cyclone.

According to the scaling arguments leading to (18) and (19), we expect the size of the anticyclone to grow with time like $t^{1/3}$ in the rotating case. Plots of the diameter of the lens based on the tracer field are in reasonable accord, except for those in which $f = 0$ which exhibit a very different, but readily understandable $t^{2/3}$ behavior consistent with Eq. 11 (Fig. 13). In the rotating case our model suggests that, in the early stages of its life, the plume grows like $t^{2/3}$ then slows down to a rate close to, but somewhat less than $t^{1/3}$, consistent with Eq. 11. Figure 13 also shows that the lateral scale to which the lens expands is essentially independent of N, as suggested by (18). However, the self-consistency of the scaling and its apparent applicability across the range of regimes over the lifetime of the plume is perhaps more convincing.

The cyclonic swirl around the stem of the plume is observed to increase steadily with time, rising to and levelling off at $u_f \sim fl_f$ (Fig. 14a). The swirl velocity of the anticyclone (Fig. 14b) is somewhat less than u_f, and its behavior led to the relationships summarized in (24). In particular, we observe the N^{-1} ordering of the velocity scale.

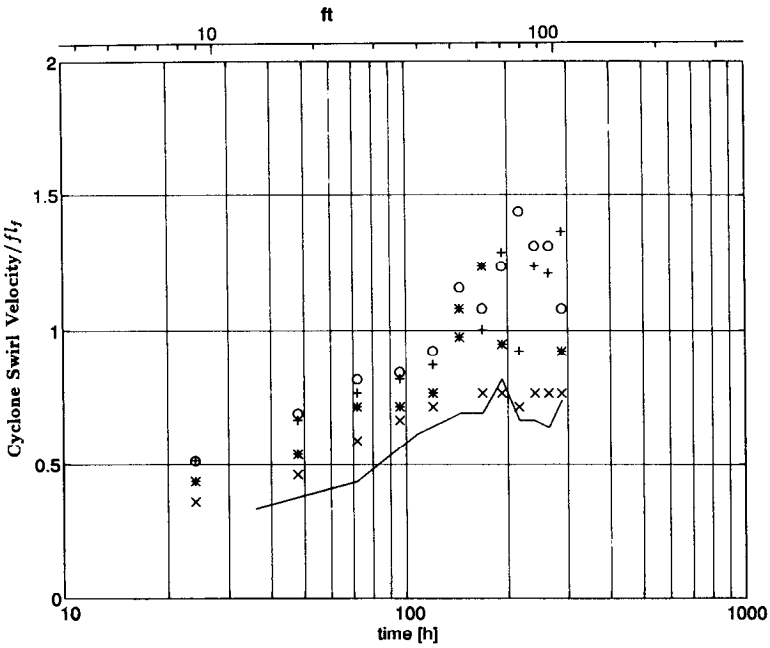

Figure 14. (a) Cyclonic swirl velocity (scaled by $u_f = fl_f$) versus time [see Table 2 for symbols].

Tracers tend to be swept up into the rising plume by entrainment, obscuring evidence of the cyclone in the tracer field. We used angular momentum surfaces to reveal some of the dynamics (Fig. 15). The contraction and expansion of angular momentum surfaces (cylinders) provides a useful measure of particle displacement. Using the maximum outward displacement for the anticyclone and the maximum inward displacement for the cyclone, the velocity in both vortices is found to obey the relation $V = f\delta r$.

In runs 6, 8, 10, 13, corresponding to a range of N from 1.5 to 4 $\times$ 10^{-4} s^{-1}, the contraction of the $m = 5$ m^2 s^{-1} surface at the bottom after 8 days was 242 $\pm$ 18 m. The resulting cyclone velocity scale $f\Delta r_c$ is 2.4 $\pm$ 0.2 cm s^{-1}, and the ratio of the maximum observed cyclonic swirl velocity to this scale 3.0 $\pm$ 0.8. In the anticyclone the measured displacement Δr ranged from 73 to 200 m. A simple fit produced an N dependence of $N^{-1.1}$, close to the expected $N^{-13/12}$ dependence (15). The observed maximum anticyclonic swirl velocities divided by $f\Delta r$ averaged 1.0 $\pm$ 0.3.

The key difference between the upper and lower vortices is the N-dependence. For the anticyclone, V and δr scale as expected from the $N^{-13/12}$ result. In the cyclone, both V and δr have no apparent N dependence, which agrees with the l_f and fl_f scaling inferred from buoyancy conservation (Figs. 14a and 15). This result for the cyclone is fundamental to the division of the plume into two vortices. The distinctive displace-

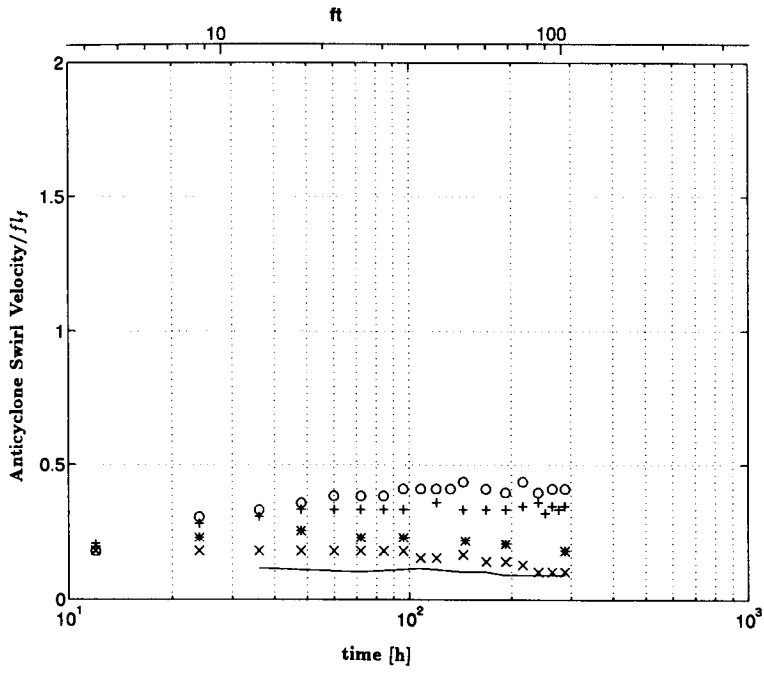

Figure 14. (b) Anticylconic swirl velocity (scaled by $u_f = fl_f$) versus time [see caption to Fig. 1 and Table 2].

ment scaling suggests a role for angular momentum surfaces in the cyclone analogous to the role isopycnals play in the anticyclone.

The Rossby number u/fl of the anticyclonic lens based on the tracer scale does not remain constant in time, but is observed to decrease as the plume expands (Fig. 16). The Rossby number is small (Section 3f), however, even after a day or so, showing that the lens is in geostrophic balance. Its vertical and horizontal scales are such that the Burger number Nh/fl is relatively constant and of order unity (Fig. 17).

One of our simulations was integrated for an extended period (run 10—see Table 2) to study the ultimate breakup of the vortex pair. After 50 days of integration the anticyclonic lens showed no signs of detaching itself from the underlying cyclone. Thus, at this time, we have no numerical confirmation of our predicted breakup scale (46 days for run 10).

5. Discussion

The addition of rotation to the classical turbulent plume problem in a stratified environment constrains the horizontal displacement of parcels. They can no longer move radially inward from great distances to fill the region evacuated by heating; parcels which undergo a limited radial displacement also turn and circulate around

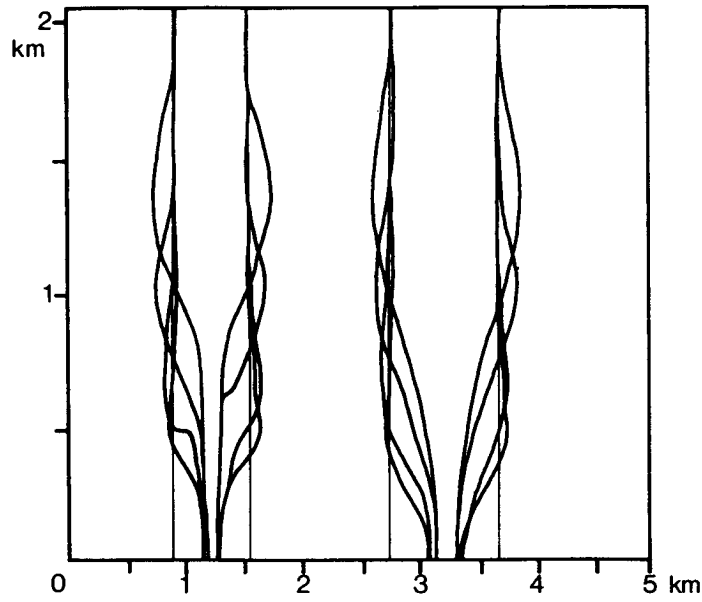

Figure 15. Cross-sections of angular momentum surfaces: 5 $m^2 s^{-1}$ (left), and 10 $m^2 s^{-1}$ (right) for runs 8, 6, 13, 10 at day 8 (in order of decreasing height). Sections are offset by 2 km for clarity.

the source. Just as the density stratification of the ocean constrains vertical excursions of fluid parcels, the horizontal 'stratification' of angular momentum surfaces constrains the horizontal excursions of parcels. An alternative perspective considers the addition of stratification to rotating convection in a neutral fluid; stratification eventually blocks the vertical penetration of the plume and shields more distant levels from the direct influence of the buoyancy source. Thus, the plume eventually divides into a spreading, anticyclonic vortex at the equilibrium level, and a converging, cyclonic vortex below. We have focussed our study on plumes whose penetration is constrained by stratification rather than a boundary, but the approach may be useful in other situations. A summary of our key scaling results is given in Figure 11 and Table 3.

In the hydrothermal problem the rotation scale l_f appears as a result of conservation of buoyancy in the cyclone and rotational confinement. Over this scale, isopycnals and angular momentum surfaces are roughly parallel. An enhanced lateral mixing can occur along these surfaces as fluid drawn inward and downward to the rising plume can freely move outward as well.

After many rotation periods the rising plume has transferred an amount of mass comparable to that within a deformation radius of the source. At this time the plume is wide enough to support unstable waves around its perimeter, and it is likely to split into vortices which propagate away from the source. Experiments with our numerical

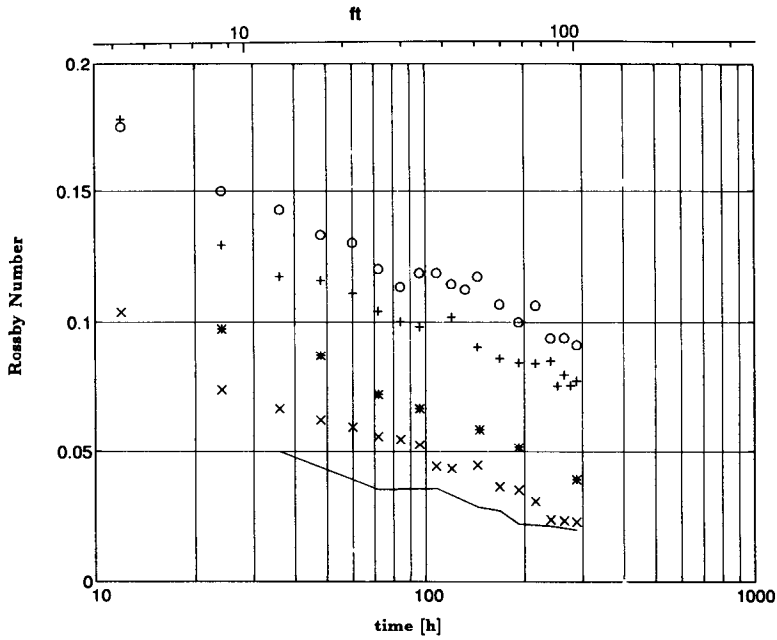

Figure 16. Rossby number u/fl in the anticyclone versus time [see caption to Fig. 1 and Table 2].

model have not yet demonstrated that this instability is in fact realized, but plumes grown in laboratory experiments (Helfrich and Battisti, 1991) do become unstable. At very long integration times the plume approaches the boundary of the domain, and the stability of our numerical plumes may be a consequence of the artificial nature of the doubly periodic boundary conditions employed; experiments are underway to address this question.

The hydrothermal plume is a highly coherent convection phenomenon, with forcing localized at a fixed point (or virtual source). Does the hydrothermal plume have any relevance to the nonlocalized forcing of a typical surface convection problem, with a specified buoyancy flux? In the flux problem, dense or buoyant convective elements are formed from boundary layer fluid exposed directly to the forcing. These elements move away from the boundary as miniature thermals, draining the boundary layer over some area comparable to the size of the elements themselves. Converging flow replaces the sinking fluid and tends to gather the elements together in a plume. The area of the plume on the boundary ought to scale as the rotation scale l_f^2, which in the case of a buoyancy flux of strength B is $l_f = (B/f^3)^{1/2}$. For equivalent scales in the flux case and the localized source case, B and F must be related thus: $B = (f^3F)^{1/2}$. The values $B = 3 \times 10^{-7}$ m^2 s^{-3}, $f = 10^{-4}$ s^{-1}, and $F = 10^{-1}$ m^4 s^{-3} are in accord with this relation and are plausible for deep convection sites as well as hydrothermal sources. In other words, plumes in deep convection

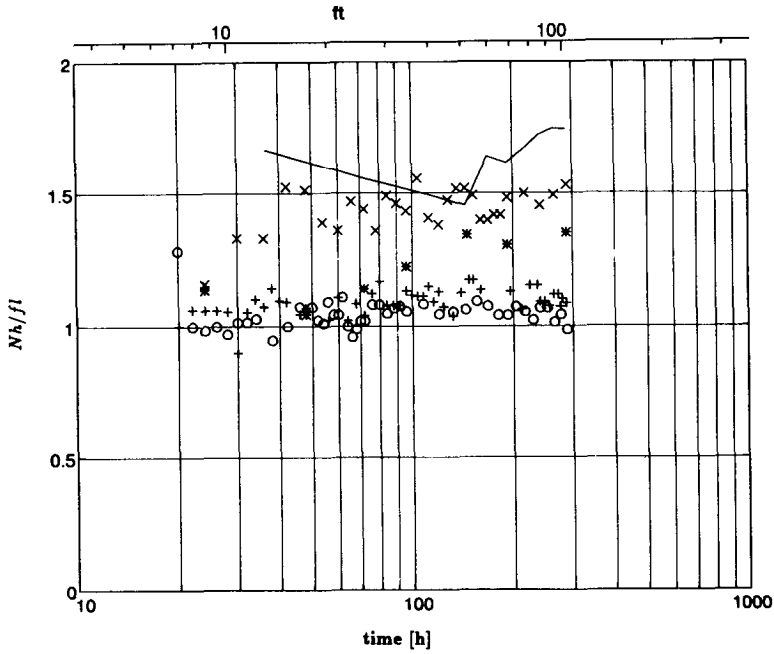

Figure 17. Scaled aspect ratio of the anticyclone Nh/fl versus time [see caption to Fig. 1 and Table 2].

draw on a buoyancy source comparable to that of hydrothermal plumes. Thus the two types of convective plumes are expected to have similar scales, and studies of hydrothermal plumes ought to help to understand the nature of oceanic convection and the associated vertical transport from the surface as well.

Acknowledgments. KGS was supported by the Centre National de la Recherche Scientifique. JM received support from the Tokyo Electric Power Company through the TEPCO/MIT research program, and also from the US Office of Naval Research. Numerous preliminary experiments were carried out at MIT by C. Hill.

APPENDIX

Model details

Our model of hydrothermal plumes is based on the non-hydrostatic equations for a Boussinesq incompressible fluid:

$$\left.\begin{aligned} \frac{Du}{Dt} + \frac{1}{\rho_o}\frac{\partial p'}{\partial x} - fv &= F_u - D_u \\ \frac{Dv}{Dt} + \frac{1}{\rho_o}\frac{\partial p'}{\partial y} + fu &= F_v - D_v \end{aligned}\right\} \tag{A.1}$$

$$\frac{Dw}{Dt} + g\frac{\rho'}{\rho_o} + \frac{1}{\rho_o}\frac{\partial p'}{\partial z} = F_w - D_w \tag{A.2}$$

$$\frac{\partial u}{\partial x} + \frac{\partial v}{\partial y} + \frac{\partial w}{\partial z} = 0 \tag{A.3}$$

$$\frac{DT}{Dt} = F_T - D_T \tag{A.4}$$

$$\frac{DC}{Dt} = F_C - D_C \tag{A.5}$$

where

$$\frac{D}{Dt} = \frac{\partial}{\partial t} + u\frac{\partial}{\partial x} + v\frac{\partial}{\partial y} + w\frac{\partial}{\partial z} \tag{A.6}$$

is the substantial derivative. Here T is the temperature, C is a tracer,[4]

$$\rho = \rho(T) \tag{A.7}$$

is assumed to be a function of temperature T alone. Here, ρ_o is a standard constant value of density and ρ' the perturbation of ρ from the initial density profile (ρ_s). The initial pressure field (p_s) is in hydrostatic balance with the initial density profile. The deviation of the pressure from p_s is p'. The velocity in the three co-ordinate directions, x pointing east, y pointing north and z vertically, are u, v and w respectively. Note that the momentum equations include Coriolis terms with a constant Coriolis parameter (f): horizontal components of the Coriolis force are not represented. Forcing and dissipation are represented symbolically, with an appropriate subscript, by F and D respectively. A schematic diagram of the model configuration is presented Figure 2.

Sub-grid-scale parameterizations and boundary conditions.

A standard 'Fickian' form has been adopted for D on the right-hand side of the momentum and thermodynamic equations, (A.1), (A.2) (A.4) and (A.5):

$$D_\Phi = -K_\Phi\left(\frac{\partial^2\Phi}{\partial x^2} + \frac{\partial^2\Phi}{\partial y^2} + \frac{\partial^2\Phi}{\partial z^2}\right). \tag{A.8}$$

Here K_Φ is a diffusion coefficient for the quantity Φ where Φ may be T, u, v or w. The diffusion is assumed to be positive and held constant in time and space.

The K's should be interpreted as eddy diffusivities and viscosities representing the turbulent transfer of properties on scales which are not resolved by the grid. The

4. If required, the effects of compressibility can be conveniently accommodated by replacing T in Eq. A.7 with potential temperature (θ) and in place of (A.4) integrating a prognostic equation forward for θ.

Laplacian form (A.8) was chosen for its simplicity. It necessitates the use of additional boundary conditions at the top and bottom of the model. We choose to set the vertical flux of horizontal momentum and heat to zero:

$$\frac{\partial \Phi}{\partial z} = 0 \tag{A.9}$$

where Φ is T, u or v. These ensure that total momentum and heat are conserved in the periodic model in the absence of imposed sources and sinks.

At the lateral boundaries of our model we adopt periodic boundary conditions; this eliminates the need for higher-order conditions or the resolution of frictional boundary layers there.

To eliminate fast-moving surface gravity waves at the upper boundary of our model we apply the rigid-lid condition

$$w = 0 \qquad \text{at } z = 0. \tag{A.10}$$

Likewise, at the flat lower boundary of the model we set:

$$w = 0 \qquad \text{at } z = -H. \tag{A.11}$$

Furthermore we assume that the upper and lower boundaries of the model are 'free' as well as impenetrable by setting the second derivative of w to zero:

$$\frac{\partial^2 w}{\partial z^2} = 0 \qquad \text{at } z = 0, -H \tag{A.12}$$

Model set-up.

Our model is initialized with a resting, linearly stratified ocean governed by an equation of state of the following form

$$\rho = \rho_o(1 - \alpha(T - T_o)) \tag{A.13}$$

where α is the coefficient of thermal expansion of water (taken to be $2 \times 10^{-4}{}^{\circ}\mathrm{C}^{-1}$) with ρ_o and T_o appropriately chosen constants.

Buoyancy gain is forced by adding an increment of temperature to the body of the fluid in a bottom boundary layer, at a rate given by the function $F_T(x, y, z, t)$ in the thermodynamic equation (A.4). All other forcing functions are set to zero. The function F_T is employed to trigger the rising plume in the bottom layer of the model; it represents the net thermodynamic effect of unresolved aspects of the plume system which distribute the warning induced by the hot vent in the boundary layer over the scale of the grid.

F_T has been chosen to have the form

$$F_T = \mathscr{F}(z) \times \mathscr{G}(x, y) \tag{A.14}$$

where, respectively, $\mathscr{F}$, $\mathscr{G}$ specify the vertical and horizontal dependence of the forcing. $\mathscr{F}$ is related to the heat-flux ($\mathscr{H}$) by

$$\left.\begin{aligned} \mathscr{F} &= \mathscr{H}/\rho_o C_p h \quad \text{for} \quad -h < z \leq 0 \\ \mathscr{F} &= 0 \quad \text{for} \quad -H \leq z \leq -h \end{aligned}\right\} \tag{A.15}$$

where $\mathscr{H}$ is in Wm^{-2}, C_p is the specific heat of water, ρ_o the mean density of seawater, and h the depth over which $\mathscr{F}$ is applied. We choose h to be the thickness of the grid-cell adjacent to the bottom boundary. Note that buoyancy flux is related to the heat-flux through

$$B_o = \frac{g\alpha\mathscr{H}}{\rho C_p} \tag{A.16}$$

where $C_p = 3900$ J $\mathrm{Kg}^{-1}\,K^{-1}$ is the specific heat of seawater.

In the experiments presented here we choose

$$\mathscr{H} = 9200\ \mathrm{Wm}^{-2}$$
$$L_x = L_y = 15\ \mathrm{km}$$
$$h = 50\ \mathrm{m};\ H = 2\ \mathrm{km}.$$

We warm over a circular patch at the bottom which has a radius of 100 m, so the choice of $\mathscr{H}$ above implies a total heat source of order 100 MW, broadly consistent with observations in the field. The (uniform) resolution of the model in all cases is $\Delta x = \Delta y = 50$ m and $\Delta z = 50$ m.

One day of integration on the $132 \times 132 \times 40$ grid, using a time-step of 60 seconds, requires 90 minutes of a single CRAY—XMP processor and 5 million words of memory.

REFERENCES

Baker, E. T., G. J. Massoth and R. A. Feely. 1987. Cataclysmic hydrothermal venting on the Juan de Fuca Ridge. Nature, *329,* 149–171.

Brugge, R., H. Jones and J. Marshall. 1991. Non-hydrostatic ocean modeling for studies of open ocean deep convection, *in* Proceedings of: Deep convection and deep-water formation in the oceans, Elsevier, Holland, 325–340.

Converse, D. R., H. D. Holland and J. M. Edmond. 1984. Flow rates in the axial hot springs of the East Pacific Rise (21°N): implications for the heat budget and the formation of massive sulfide deposits. Earth Planet. Sci. Lett., *69,* 159–175.

Crane, K., F. Aikman III, R. Embley, S. Hammond, A. Malahoff and J. Lupton. 1985. The distribution of geothermal fields on the Juan de Fuca Ridge. J. Geophys. Res., *90* (B1), 727–744.

Fernando, H. J. S., D. Boyer and R-R. Chen. 1989. Turbulent thermal convection in rotating and stratified fluids. Dyn. Atmos. Oceans, *13,* 95–121.

Gill, A. E. 1981. Homogeneous intrusions in a rotating stratified fluid. J. Fluid Mech., *103,* 275–296.

Hedstrom, K. and L. Armi. 1988. An experimental study of homogeneous lenses in a stratified rotating fluid. J. Fluid Mech., *191,* 535–556.

Helfrich, K. R. 1994. Thermals with background rotation and stratification. J. Fluid Mech., *259,* 265–280.

Helfrich, K. R. and D. Battisti. 1991. Experiments on baroclinic vortex shedding from hydrothermal plumes. J. Geophys. Res., *96,* 12511–12518.

Helfrich, K. R. and U. Send. 1988. Finite amplitude evolution of two-layer geostrophic vortices. J. Fluid Mech., *197,* 331–348.

Hopfinger, E. J., F. K. Browand and Y. Gagne. 1982. Turbulence and waves in a rotating tank. J. Fluid Mech., *125,* 505–534.

Jones, H. and J. Marshall. 1993. Convection with rotation in a neutral ocean; a study of open-ocean deep convection. J. Phys. Oceanogr., *23,* 1009–1039.

Joyce, T. M. and K. G. Speer. 1987. Modeling the large-scale influence of geothermal sources on abyssal flow. J. Geophys. Res., *92* (C3), 2843–2850.

Lavelle, J. W. 1994. A convection model for hydrothermal plumes in a cross flow. NOAA Technical Memorandum ERL PMEL-102, Pacific Marine Environmental Laboratory, Seattle, WA, 18 pp.

Legg, S. and J. Marshall. 1993. A heton model of the spreading phase of open-ocean deep convection. J. Phys. Oceanogr., *23,* 1041–1056.

Little, S. A., K. D. Stolzenbach and R. P. Von Herzen. 1987. Measurements of plume flow from a hydrothermal vent field. J. Geophys. Res., *92,* 2587–2596.

Lupton, J. E., J. R. Delaney, H. P. Johnson and M. K. Tivey. 1985. Entrainment and vertical transport of deep-ocean water by buoyant hydrothermal plumes. Nature, *316,* 621–623.

Marshall, J., J. Whitehead and T. Yates. 1994. Laboratory and numerical experiments in ocean convection, *in* Ocean Processes in Climate Dynamics: Global and Mediterranean Examples, P. Melanotte-Rizzoli and A. R. Robinson, eds., Kluwer Academic Publishers, Netherlands, 173–201.

Maxworthy, T. and S. Narimousa. 1994. Unsteady, turbulent convection into a homogeneous, rotating fluid, with oceanographic applications. J. Phys. Oceanogr., *24,* 865–887.

McWilliams, J. C. 1988. Vortex generation through balanced adjustment. J. Phys. Oceanogr., *18,* 1178–1192.

McWilliams, J. C., P. R. Gent and N. J. Norton. 1986. The evolution of balanced, low-mode vortices on the β-plane. J. Phys. Oceanogr., *16,* 838–855.

Middleton, J. H. 1986. The rise of plumes in a stably stratified crossflow. Boundary-Layer Meteor., *36,* 187–199.

Pedlosky, J. 1985. The instability of continuous heton clouds. J Atmos. Sci., *42,* 1477–1486.

Sclater, J. G. and J. Francheteau. 1970. The implications of terrestrial heat flow observations on current tectonic and geochemical models of the crust and upper mantle of the Earth, *in* Plate Tectonics and Geomagnetic Reversals, A. Cox, editor. W. H. Freeman and Co., San Francisco.

Sclater, J. C., C. Jaupart and D. Galson. 1980. The heat flow through the oceanic and continental crust and the heat loss of the earth. Rev. Geophys. Space Phys., *18*(1), 269–311.

Speer, K. G. 1989. A forced baroclinic vortex around a hydrothermal plume. Geophys. Res. Lett., *16*(5), 461–464.

Speer, K. G. and P. A. Rona. 1989. A model of an Atlantic and Pacific hydrothermal plume. J. Geophys. Res., *94*(C5), 6213–6220.

Stommel, H. 1982. Is the South Pacific helium-3 plume dynamically active? Earth Planet. Sci. Lett., *61,* 63–67.

Stone, P. H., 1968. Some properties of Hadley regimes on rotating and non-rotating planets. J. Atmos. Sci., *25,* 664–657.

Thorpe, A. J. and R. Rotunno. 1989. Nonlinear aspects of symmetric instability. J. Atmos. Sci., *46,* 1285–1299.

Turner, J. S. 1973 Buoyancy Effects in Fluids., Cambridge University Press, London, 367 pp.

—— 1986 Turbulent entrainment: the development of the entrainment assumption and its application to geophysical flows. J. Fluid Mech., *173,* 431–471.

Received *20 November 1994;* revised: *13 June, 1995.*